Effect of the Substrate Position and Flow Rate Ratio on the Properties of a-C:H Films Deposited by Pseudo-Spark Discharge Plasma CVD Using Acetylene and Ar

Takaharu KAMADA[1)]*, Yuto TSUKIDATE[2)], Masayuki WATANABE[3)], Yoshitaka NAKAMURA[1)], Seiji MUKAIGAWA[4)]

[1)] *Industrial Systems Engineering Department, National Institute of Technology (KOSEN), Hachinohe College, Aomori 039-1192, Japan*
[2)] *Industrial Systems Engineering Advanced Department, National Institute of Technology (KOSEN), Hachinohe College, Aomori 039-1192, Japan*
[3)] *Institute of Quantum Science, Nihon University, Tokyo 101-8308, Japan*
[4)] *Faculty of Science and Engineering, Iwate University, Iwate 020-8551, Japan*

(Received 27 May 2025 / Accepted 10 December 2025)

Hydrogenated amorphous carbon (a-C:H) films were deposited on silicon wafers using a pseudo-spark discharge (PSD) method. A mixture of argon and acetylene (C_2H_2) was employed as the process gas. PSD generates high-density plasma and forms a diffuse discharge due to the hollow cathode effect. The film structure was analyzed using Raman spectroscopy, while film hardness was measured using nanoindentation. Surface hybridization states and contamination levels were examined by X-ray photoelectron spectroscopy. This study investigates the optimal distance between the anode and the deposition substrate, as well as the optimal flow rate ratio using acetylene diluted with argon. The results indicated that the optimal substrate distance was 40 mm and the ideal flow rate ratio ($Ar/(Ar + C_2H_2)$) was 1%. Under these conditions, the a-C:H films exhibited a G-band position of 1,571 cm^{-1}, a full width at half maximum of 114 cm^{-1} for the G peak, a deposition rate of 155 nm/h, and a hardness of 5.3 GPa.

Keywords: Hydrogenated amorphous carbon (a-C:H) film, pseudo-spark discharge (PSD), Raman spectrum, film hardness

DOI: 10.1585/pfr.21.1406014

1. Introduction

Hydrogenated amorphous carbon (a-C:H) films are amorphous carbon coatings composed of a mixture of sp^3- and sp^2-hybridized carbon and hydrogen atoms [1, 2]. These films exhibit desirable properties such as low friction coefficients, high mechanical hardness, chemical inertness, and optical transparency [3–6]. Due to these characteristics, a-C:H films find applications in various fields, including manufacturing, medical devices, electronics, and the aerospace industry [7–9]. Plasma-enhanced chemical vapor deposition (CVD) is one of the primary techniques for depositing a-C:H films. Various CVD methods have been employed, such as radio frequency plasma [10], plasma ion implantation [11], and electron cyclotron resonance plasma [12], with the selection of the plasma source tailored to specific coating requirements.

In this study, pseudo-spark discharge (PSD) [13, 14] was used as the plasma source for depositing a-C:H films [15, 16]. PSD is a type of gas discharge that occurs at low pressure, to the left of the minimum on the Paschen curve, and utilizes a specialized electrode structure [17]. The PSD electrode assembly comprises two parallel plate electrodes, each with a central hole, and the cathode incorporates a cylindrical cavity (hollow cathode) behind the hole. The typical electrode spacing in PSD systems is 3–5 mm. At these low pressures, the electron mean free path becomes comparable to or longer than the electrode spacing, allowing the initial discharge to propagate through the central holes. During PSD operation, an electron avalanche is triggered by secondary electrons generated from ion impact and photoelectron emission, resembling a Townsend discharge. As the discharge progresses, a positive space charge accumulates near and within the cathode hole, enhancing the electric field's penetration into the hollow cathode. This intensifies the oscillatory motion of electrons and promotes photoelectron emission, making γ-induced emission the dominant mechanism. Consequently, a highly ionized diffuse plasma is formed [18]. The PSD's ability to produce high-density plasma enables high deposition rates and maintains a glow-like discharge between the electrodes, even at high current, thereby preventing thermal discharge and suppressing particle contamination. These advantages eliminate the need for particle removal systems using magnetic fields

*Corresponding author's e-mail: kamada-e@hachinohe-ct.ac.jp

or electrode cooling, allowing for a simpler deposition system.

In previous work, the authors deposited a-C:H films on silicon substrates using a CH_4/H_2 gas mixture, achieving a maximum film hardness of approximately 2.6 GPa [19]. High hardness is critical for many applications, and it is known to depend on the choice of precursor gas. Lai *et al.* reported that films deposited using a C_2H_2/Ar mixture exhibited superior mechanical properties compared to those obtained with CH_4/Ar [20]. In this study, a-C:H films were deposited on silicon substrates using a mixture of C_2H_2 and Ar as the process gas. The influence of deposition parameters—specifically, substrate position and the mixing ratio of Ar in the process gas—on the structural and mechanical properties of the a-C:H films was investigated.

2. Experimental Details

Figure 1 shows a schematic diagram of the experimental setup used in this study. The vacuum chamber, made of stainless steel and equipped with multiple measurement ports, has a diameter of 26.7 cm and a height of 51.8 cm. The chamber was evacuated to approximately 4×10^{-4} Pa using an oil diffusion pump. For the PSD electrode assembly, both the cathode—denoted as HC in the figure—and the anode (A) were made of molybdenum. The hollow cavity of the HC, however, was fabricated from stainless steel. Each electrode had a thickness of 2 mm. The cathode and anode holes had diameters of 5 and 10 mm, respectively. The HC cavity was 50 mm deep with an internal diameter of 40 mm. The interelectrode distance (d) was set to 5 mm using spacers made of Teflon (diameter: 60 mm) and ceramics (diameter: 10 mm). The HC was connected to a stainless-steel tube, which served both as a conduit for introducing process gas into the hollow electrode and for applying a negative voltage to the HC. The anode was electrically grounded.

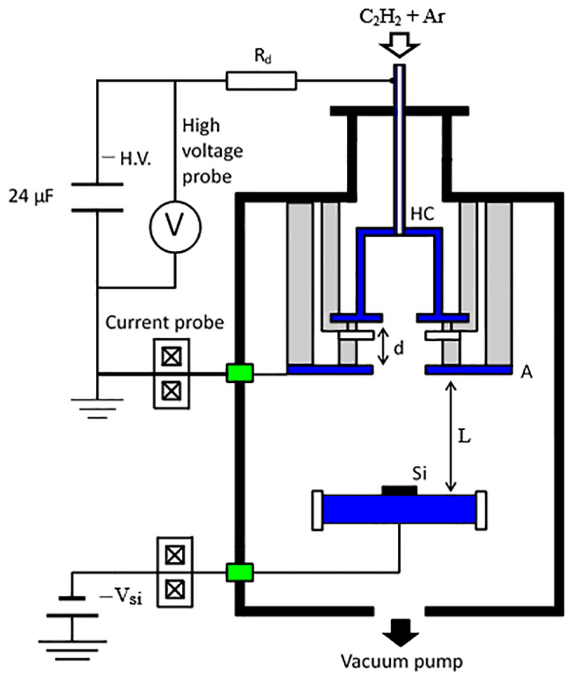

Fig. 1. Schematic diagram of the PSD PE-CVD deposition system.

The substrates used were (100)-oriented silicon wafers with a thickness of 0.5 mm. Prior to deposition, the substrates were ultrasonically cleaned in ethanol and acetone. Each substrate was mounted on a 70 mm square stainless-steel holder placed downstream from the plasma relative to the anode. The distance between the substrate holder and the anode (L) was varied from 30 to 60 mm. The surface temperature of the substrate holder was approximately 170°C. Before deposition, the substrates were sputter-cleaned in an Ar and H_2 plasma at a substrate bias voltage (V_{si}) of −100 V.

For the deposition process, a mixture of C_2H_2 and Ar gases was used as the process gas. Gas flow rates were measured using a mass flow sensor (Alicat M series) and controlled via a needle valve. The Ar flow rate ratio was varied at 0.5%, 1%, 5%, 10%, and 30%. Due to the flow sensor's precision, the total gas flow rate was set to 2 mL/min for 0.5% Ar, 1 mL/min for 1% Ar, and 0.5 mL/min for the remaining ratios. The deposition pressure was maintained at approximately 16 Pa, regulated by the exhaust valve of the vacuum pump. A 24 μF capacitor bank was slowly charged up to approximately −2.4 kV. Once the cathode potential reached the breakdown voltage, spontaneous discharge occurred. A non-inductive 1.2 Ω resistor was included in the discharge circuit. Film deposition was performed under a substrate bias voltage (V_{si}) of −150 V. Each experiment consisted of 800 discharge shots, with a discharge interval of about 10 s. The deposition rate was calculated based on the measured film thickness, assuming a total discharge duration of 8,000 s. After film deposition, the chamber was filled with H_2 and allowed to cool naturally.

The discharge current was measured with a Rogowski coil, and the breakdown voltage was measured with a high-voltage meter. For analysis and observation of deposited films, a laser micro-Raman spectrometer (Renishaw inVia, laser wavelength: 532 nm) was used to determine the structure of the films, a nanoindentation hardness tester (Elionix ENT-1100a, maximum load: 0.1 mN, maximum indentation depth: 20 nm) was used to measure the film hardness, and an X-ray photoemission spectrometer (KRATOS AXIS-NOVA) was used to analyze the chemical composition. The deposition rate was estimated using cross-sectional images taken with a scanning electron microscope (JEOL JSM7100F).

3. Experimental Results

3.1 Typical discharge waveform

Figure 2 shows the typical discharge current and voltage waveforms between the electrodes at an argon mixing ratio of 5%. The oscillation of the voltage between the PSD electrodes was suppressed by incorporating a non-inductive resistor (R_d) into the circuit. The breakdown voltage was approximately −2.4 kV, and the peak discharge current reached about 4.5 kA. The main sustained discharge duration was approximately 25 μs. Similar waveforms were observed across all

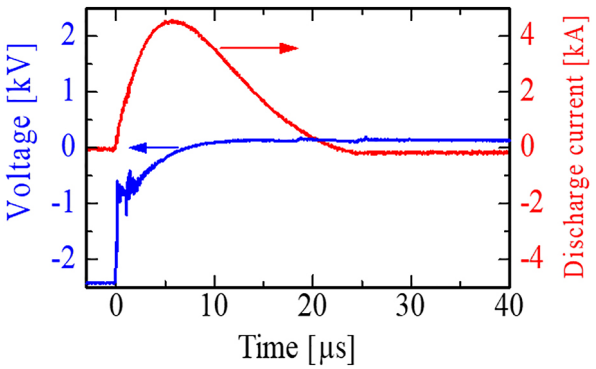

Fig. 2. Typical waveforms for discharge current and voltage between electrodes.

tested gas flow ratios, indicating stable discharge characteristics under varying conditions.

3.2 Substrate distance

The influence of substrate distance (L) on the properties of the deposited films was examined at an Ar flow rate ratio of 5%. Figure 3 presents the typical Raman spectra of films deposited at different substrate distances. The Raman spectra of the films displayed two broad bands in the range of 1,000–1,800 cm^{-1}: the G-band peak near 1,580 cm^{-1} and the D-band peak near 1,350 cm^{-1} [21]. The dashed line in the figure represents the baseline due to the fluorescent component of hydrogen. The slope of this baseline correlates with the hydrogen content in the film. The approximate hydrogen concentration can be estimated using the following equation [22].

$$\mathrm{H\ [at.\ \%]} = 21.7 + 16.6 \log\left\{\frac{m}{I(\mathrm{G})}\ [\mu\mathrm{m}]\right\}, \quad (1)$$

where m is the slope of the baseline and I(G) is the emission intensity of the G peak. The value of m/I(G) increases exponentially with hydrogen concentration. At substrate distances of 30, 40, 50, and 60 mm, the corresponding m/I(G) values were 1.8, 2.0, 5.8, and 8.1, respectively, indicating higher hydrogen incorporation in the films deposited at 50 and 60 mm. This increase is likely due to a reduced sputtering effect from ions at longer distances. It should be noted that m/I(G) is sensitive to photoluminescence quenching processes and has been reported to have low sensitivity to hydrogen bonded to sp^2 carbon [23]. Therefore, in this study, m/I(G) is interpreted as indicating a trend in hydrogen concentration, but it is not used for quantitative evaluation of hydrogen content.

To further investigate the structural characteristics of the films, Raman spectra from L = 30 and 40 mm (with relatively low hydrogen content) were analyzed. Figure 4 shows the baseline-corrected Raman spectrum and its deconvolution into G and D peaks for the film deposited at L = 40 mm. The following parameters were evaluated: G peak position (G-position), full width at half maximum of the G peak (FWHM(G)), and the area ratio of the D and G peaks (I(D)/I(G)). Each value represents the average from 12 locations on the film surface. A lower G-position and I(D)/I(G) ratio are

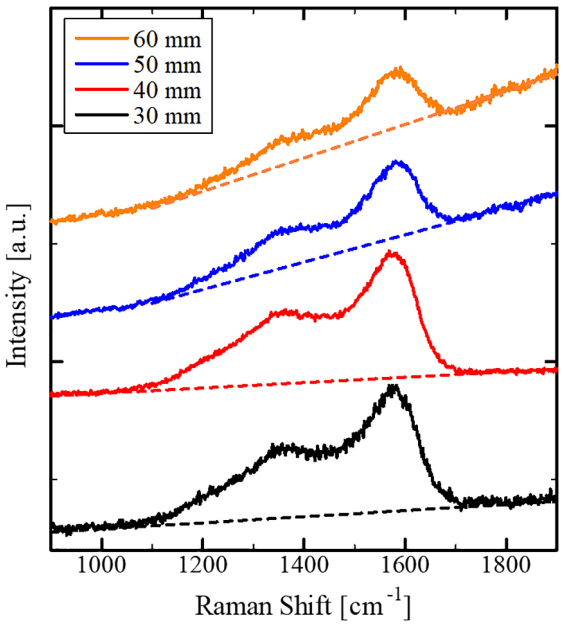

Fig. 3. Raman spectra of a-C:H films deposited at various substrate distances (L = 30–60 mm) under an Ar flow rate ratio of 5%. The dashed lines represent the baseline used to evaluate the hydrogen content in the films.

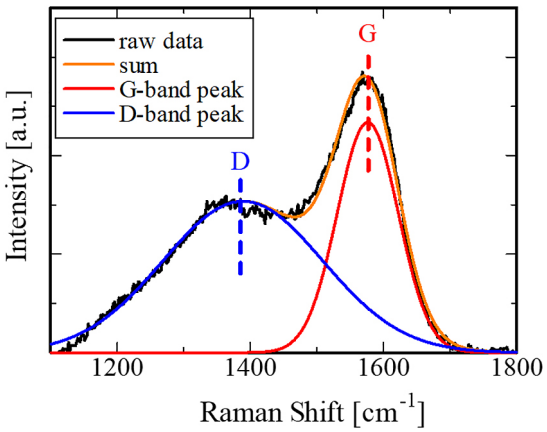

Fig. 4. Typical Raman spectrum of the two-peak separation analysis for L = 40 mm.

indicative of a higher sp^3 content, while a broader FWHM(G) suggests increased bond disorder [21]. However, it is well known that each parameter in Raman spectroscopy is influenced by multiple factors, such as the size of sp^2 clusters, structural disorder, and hydrogen content [24]. Therefore, it is difficult to quantitatively determine detailed structural changes in the film based solely on the features of the Raman spectra. It should be noted that the interpretation of the Raman spectra in this study is based on a qualitative inference, assuming that the film corresponds to "Stage 2" structure in the amorphous carbon model proposed by Ferrari *et al.* [21].

The measured parameters from the Raman spectra are summarized in Table 1. The values were nearly identical for L = 30 and 40 mm, indicating that both the sp^3 fraction and the degree of amorphousness were comparable between the two films.

Figure 5 shows the variation of deposition rate and film hardness as a function of substrate distance (L). The deposition rate was determined from cross-sectional SEM images by measuring the film thickness at five different points. The film thickness at L = 50 mm was the lowest, measured at approximately 240 nm. Given that the maximum indentation depth by the nanoindenter was 20 nm, the influence of substrate hardness is considered negligible. Film hardness was measured at 16 locations on the surface; the average value is reported, with error bars indicating the maximum and minimum values. The highest deposition rate and film hardness were observed at L = 40 mm, with values of 155 nm/h and 4.1 GPa, respectively. The decrease in hardness at L = 50 and 60 mm is attributed to increased hydrogen concentration in the films, as indicated by the m/I(G) values. At L = 30 mm, a reduction in film hardness was also observed. However, the Raman parameters for L = 30 and 40 mm were nearly identical, as shown in Table 1. While the m/I(G) value at L = 30 mm was the lowest, indicating a lower hydrogen content in the film, the reduction in hardness may instead be attributed to a decrease in film density. This is possibly due to enhanced ion sputtering and stronger dissociation of the process gas at shorter substrate distances.

3.3 Ar flow rate ratio in the process gas

Films were deposited with a fixed substrate distance of L = 40 mm while varying the argon (Ar) flow rate ratio between 0.5 and 30% in the C_2H_2/Ar process gas mixture. Figure 6 shows the variation of Raman parameters, deposition rate, and film hardness as a function of the Ar flow rate ratio. The G-position and I(D)/I(G) ratio decreased, and the FWHM(G) increased as the Ar flow rate ratio was reduced from 30%. These results suggest that lowering the Ar flow rate enhances the amorphization of the films and increases their sp^3 carbon content. However, at 0.5% Ar, while the G-position and FWHM(G) remained nearly constant, the I(D)/I(G) ratio was higher. This may be attributed to an increase in the area of the D-band peak, which intensifies when the crystallinity of graphitic carbon is disrupted [24]. Such disruption likely results from an increase in small, disordered sp^2 clusters due to weaker acetylene dissociation at lower Ar concentrations. The highest deposition rate was observed at an Ar flow rate-ratio of 1%, reaching 173 nm/h. This enhancement is likely due to reduced ion sputtering as the Ar concentration decreases from 30 to 1%. However, at 0.5% Ar, further reduction in ionization may have resulted in a lower deposition rate. The maximum film hardness, 5.3 GPa, was also achieved at 1% Ar. These findings show a relatively good correlation between film hardness and Raman parameters.

3.4 Film analysis by X-ray photoelectron spectroscopy

Figure 7 shows the X-ray photoelectron spectroscopy (XPS) spectrum of the carbon C1s core level for a film deposited at L = 40 mm with 1% Ar. The C1s spectrum was deconvoluted into three components to estimate the sp^3 fraction

Table 1. Results of G-position, FWHM(G) and I(D)/I(G) ratio for deposited films at L = 30 and 40 mm.

L [mm]	G-position [cm^{-1}]	FWHM(G) [cm^{-1}]	I(D)/I(G) ratio
30	1,577.0	107.3	1.862
40	1,576.2	107.2	1.865

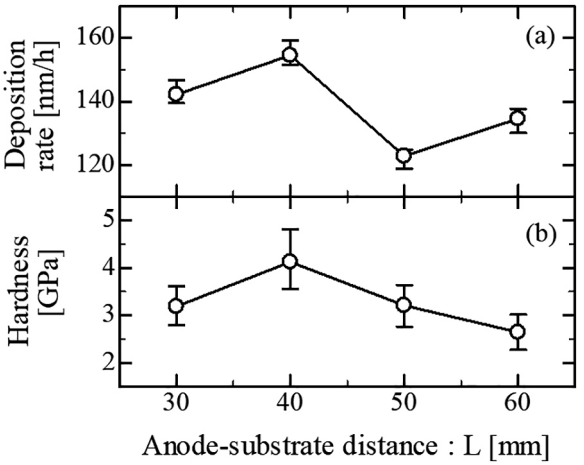

Fig. 5. (a) Deposition rate and (b) film hardness with respect to the distance L.

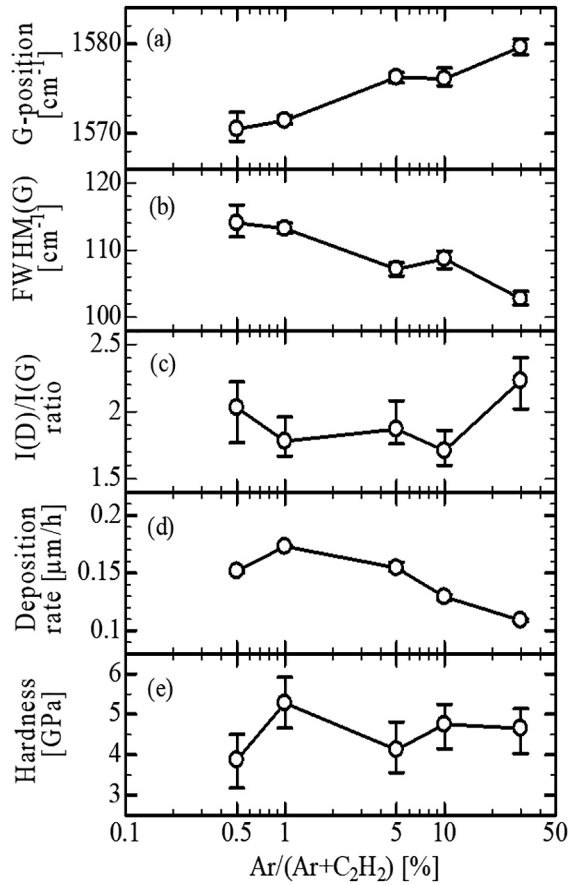

Fig. 6. (a) G-position, (b) FWHM(G), (c) I(D)/I(G) ratio, (d) deposition rate, and (e) hardness with respect to the flow rate of Ar.

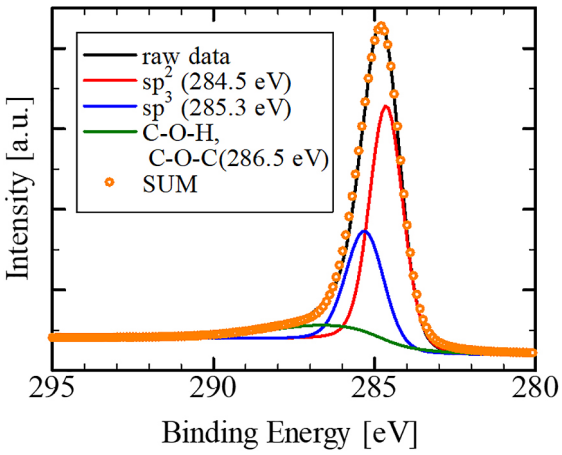

Fig. 7. C1s XPS spectrum of the a-C:H film (L: 40 mm, flow ratio rate of Ar: 1%).

Table 2. Values of sp^3 content for Ar flow rate ratio at 0.5, 1 and 5%.

Ar flow rate ratio	0.5%	1%	5%
sp^3 content	21%	35%	18%

in the film. The dominant peak at a binding energy of 284.5 eV corresponds to C=C bonds in sp^2-hybridized graphitic carbon. The peak at 285.3 eV is attributed to C-C bonding in sp^3-hybridized (diamond-like) carbon. The peak near 286.5 eV corresponds to C-O bonds, likely originating from residual oxygen in the deposition environment [12]. The sp^3 content was determined from the peak area ratio $sp^3/(sp^2 + sp^3)$, and the results are summarized in Table 2. The sp^3 content was highest at 1% Ar, whereas lower values were obtained at 0.5 and 5%. This tendency is consistent with the hardness variation shown in Fig. 6(e). Therefore, these results indicate that the highest hardness obtained at 1% Ar is partly attributed to the increased relative proportion of sp^3-bonded carbon in the film. However, it has been reported that the C1s spectrum in XPS can be decomposed into several components such as C-H and C-O depending on the deposition environment, making it difficult to accurately determine the sp^3/sp^2 ratio [21]. Therefore, the sp^3/sp^2 ratio of XPS is treated as an approximate value.

4. Conclusion

In this study, the effects of substrate distance and argon flow rate ratio in the process gas on the properties of a-C:H films deposited by PSD plasma CVD were investigated. Films were deposited on silicon substrates using a C_2H_2/Ar gas mixture under a substrate bias of 150 V.

The results demonstrated that hydrogen concentration in the films varied significantly with substrate distance. Although the Raman spectral characteristics of films deposited at 30 and 40 mm were nearly identical, a notable difference in hardness was observed, suggesting that factors such as film density or plasma-surface interactions may play a role. Further analysis, including plasma diagnostics and film density evaluation, will be necessary to clarify this. As the Ar flow rate ratio decreased, Raman spectra indicated a trend toward increased sp^3 content. XPS measurements were also conducted for films deposited with Ar flow ratios of 0.5–5%. The results showed that the sp^3 content reached its maximum value of 35% at 1% Ar, at which the film also exhibited the highest hardness of 5.3 GPa. This process condition resulted in higher film hardness than that obtained using CH_4/H_2 as process gases, demonstrating the effectiveness of the C_2H_2/Ar mixture in achieving superior mechanical properties.

Compared with the previous study using CH_4/H_2 gas mixtures [19], the film hardness obtained using C_2H_2/Ar was more than twice as high. This difference may be caused by differences in the molecular structure of the precursor gases and the chemical reactivity of the dilution gases. Therefore, comparison of the absolute values of Raman parameters should be interpreted carefully. However, important trends can be observed:

• G peak position (from 1,573.3 to 1,571.4 cm^{-1}) and FWHM(G) (from 116.1 to 113.2 cm^{-1}) showed only minor differences, suggesting similar bond disorder.

• The $I(D)/I(G)$ ratio increased significantly (from 1.21 to 1.78), indicating the growth of graphitic sp^2 clusters and suggesting a denser carbon network.

• The $m/I(G)$ value decreased (from 2.0 to 1.0), implying a reduction in hydrogen content.

These results suggest that C_2H_2-based deposition promoted the formation of a denser sp^2/sp^3 hybrid carbon structure with reduced hydrogen content maintaining the sp^3 fraction. As a result, the film density was enhanced, leading to the significant increase in hardness.

[1] S. Aisenberg and R. Chabot, J. Appl. Phys. **42**, 2953 (1971).
[2] J. Robertson, Mater. Sci. Eng. R. **37**, 129 (2002).
[3] A. Tyagi *et al.*, Int. J. Refract. Met. Hard Mater. **78**, 107 (2019).
[4] S. Kowalski, Wear **486–487**, 204076 (2021).
[5] D. Das and A. Banerjee, Appl. Surf. Sci. **345**, 204 (2015).
[6] R. Hauert, Diam. Relat. Mater. **12**, 583 (2003).
[7] S. Bhowmick and A.T. Alpas, Int. J. Mach. Tools Manuf. **48**, 802 (2008).
[8] B. Rothammer *et al.*, Polymers **13**, 1952 (2021).
[9] A. Vanhulsel *et al.*, Tribol. Int. **40**, 1186 (2007).
[10] S.I. Hosseini *et al.*, Thin Solid Films **519**, 3090 (2011).
[11] R. Hatada *et al.*, Surf. Coat. Technol. **156**, 322 (2014).
[12] R.M. Dey *et al.*, Curr. Appl. Phys. **8**, 6 (2008).
[13] J. Christiansen and C. Schultheiss, Z. Phys. **A290**, 35 (1979).
[14] W. Hartmann and M.A. Gundersen, Phys. Rev. Lett. **60**, 2371 (1988).
[15] T. Kamada *et al.*, Jpn. J. Appl. Phys. **53**, 068006 (2014).
[16] T. Kamada *et al.*, Jpn. J. Appy. Phys. **44**, 6747 (2005).
[17] K. Taguchi *et al.*, Jpn. J. Appl. Phys. **35**, 6259 (1996).
[18] M. Stetter *et al.*, IEEE Trans. Plasma Sci. **23**, 283 (1995).
[19] T. Kamada *et al.*, ICRP-11/GEC 2022, HT4.00075, Sendai, Japan (2022).
[20] K.H. Lai *et al.*, Diam. Relat. Mater. **10**, 1862 (2001).
[21] J. Robertson, Mater. Sci. Eng. R **37**, 129 (2002).
[22] C. Casiraghi *et al.*, Phys. Rev. B **72**, 085401 (2005).
[23] C. Pardanaud *et al.*, Diam. Relat. Mater. **34**, 100 (2013).
[24] A.C. Ferrari and J. Robertson, Phys. Rev. B **61**, 14095 (2000).